JACS
JOURNAL OF THE AMERICAN CHEMICAL SOCIETY
pubs.acs.org/JACS
Article

Ouroboros: From Linear Carbons to Cyclic Carbons, Cyclo[25]carbon and Cyclo[50]carbon

Yuan Guo,[†] Ling Hua,[†] Yuzhe Yun, Guorui Xu, Luye Sun,* and Wei Xu*

Cite This: https://doi.org/10.1021/jacs.6c00225
Read Online
ACCESS | Metrics & More | Article Recommendations | Supporting Information

ABSTRACT: Carbon allotropes composed solely of sp-hybridized carbon atoms, namely, linear and cyclic carbons (C_n), represent a unique class of materials with fascinating chemical structures and long-debated stability among their various isomers. Early gas-phase experiments and theoretical calculations have both suggested that for larger C_n ($n \geq 10$), the cyclic form could be more stable than the linear one. This implies that linear C_n could, in principle, serve as a precursor for the formation of cyclic carbons. Recently, on-surface synthesis has enabled the generation of a series of linear and cyclic carbons (up to cyclo[30]carbon). However, a direct structural transformation from linear to cyclic carbon has not yet been achieved in real space. Here, we present a new strategy to generate cyclic carbons from linear ones, inspired by the ancient symbol "Ouroboros", a snake eating its own tail. Using linear C_5 as a precursor (derived from C_5Br_6) and tip-induced coupling reactions, we achieved the on-surface generation of an odd-numbered cyclic carbon, C_{25}. Electronic characterization and calculations reveal that C_{25} adopts an open-shell configuration. To demonstrate the generality of this strategy, we employed linear C_6 (derived from C_6Br_6) as the precursor, which led to the formation of the largest cyclocarbon so far, C_{50}, on the surface, and importantly, its first and second ion resonances at two voltage polarities were probed successfully. Our work demonstrates a long-predicted strategy for the synthesis of cyclic carbons.

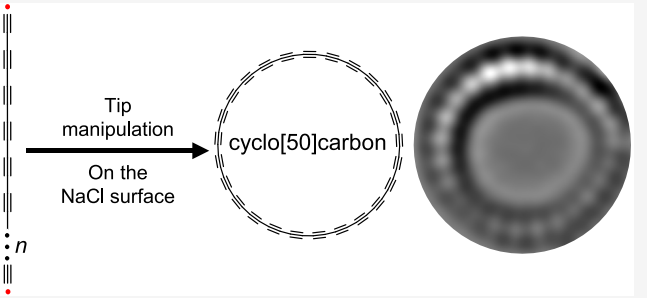

INTRODUCTION

Sp-hybridized carbon allotropes,[1−11] including linear and cyclic carbons (C_n), have long been predicted to possess remarkable properties such as exceptional mechanical strength and tunable electronic gaps.[12−18] However, their extreme reactivity has hindered their isolation as well as structural and electronic characterization.[12,19−23] With the advancement of on-surface synthesis method, a series of cyclic carbons[24−32] have been successfully synthesized via different strategies, i.e., decarbonylation/dehalogenation on macrocyclic precursors,[24,28,30] dehalogenation and retro-Bergman reactions on fully halogenated precursors,[25,27,29] and coupling and ring-opening reactions of small cyclic carbon.[31] In addition, through tip-induced coupling reactions of short linear C_5 and C_6,[33] various longer linear carbons have also been generated on surface.

Previous studies have shown that for smaller C_n ($n < 10$), the linear chain configuration is energetically favored, whereas for larger C_n ($n \geq 10$), the cyclic configuration becomes more stable.[18,21,34−41] Thus, linear C_n could be precursors for the generation of cyclic carbons.[42] Interestingly, this strategy resonates with the ancient symbol "Ouroboros", a snake eating its own tail. A famous related story is that the German chemist August Kekulé conceived the ring structure of benzene after envisioning the Ouroboros. Thus, Ouroboros motivated us to pursue the generation of cyclic carbons directly from linear carbons, which has not been achieved so far.

We chose linear C_5 (derived from C_5Br_6) as the precursor. Here, by optimizing experimental conditions, we successfully generated an odd-numbered cyclic carbon, C_{25}, directly through a tip-induced coupling reaction of linear C_5 chains (Figure 1). High-resolution atomic force microscopy (AFM) imaging directly resolves its unique hybrid cumulene-polyyne structure and identifies its open-shell structure[43] by frontier orbital imaging by scanning tunneling microscopy (STM) combined with calculations. Further bromination of C_{25} can lead to the formation of open-shell doublet $C_{25}Br$. Using a longer linear carbon, C_6, we further achieved the formation of an even larger cyclocarbon, C_{50}, the largest cyclocarbon generated on the surface to date (Figure 1), whose first and second ion resonances at both voltage polarities were experimentally probed, which was also considered to be a big challenge before.

Received: January 5, 2026
Revised: March 27, 2026
Accepted: March 30, 2026

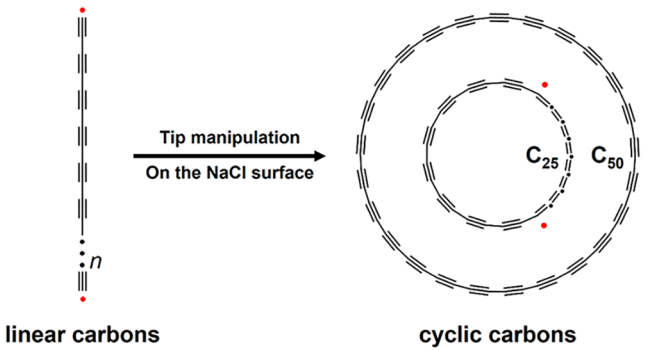

Figure 1. Schematic illustration of the formation of cyclic C_{25} and C_{50} from linear carbons on the NaCl surface.

RESULTS AND DISCUSSION

The C_5Br_6 molecules were deposited on a cold NaCl/Au(111) surface with a molecular coverage of ~0.4 monolayer (Figure 2b). Applying bias voltages of ~4.5 to 5.0 V to C_5Br_6 can induce dehalogenation, ring-opening, and coupling reactions, resulting in the formation of several linear carbons in the first step (Figure 2c). Further applying bias voltages to these linear carbons can lead to the formation of a cyclic carbon (Figure 2d), which was later identified to be a C_{25}. High-resolution AFM and Laplace-filtered images (Figures 2f–h, and S1) reveal a hybrid structure: one segment exhibits characteristic bright features of triple bonds, while the other part appears to be more uniform. This structure is sensitive to the adsorption site and can be transformed into a fully polyynic structure with 12 triple bonds and a kink site (Figure S2), like the case of C_{13}.[25] We thus assign this cyclocarbon to the cyclic C_{25}.

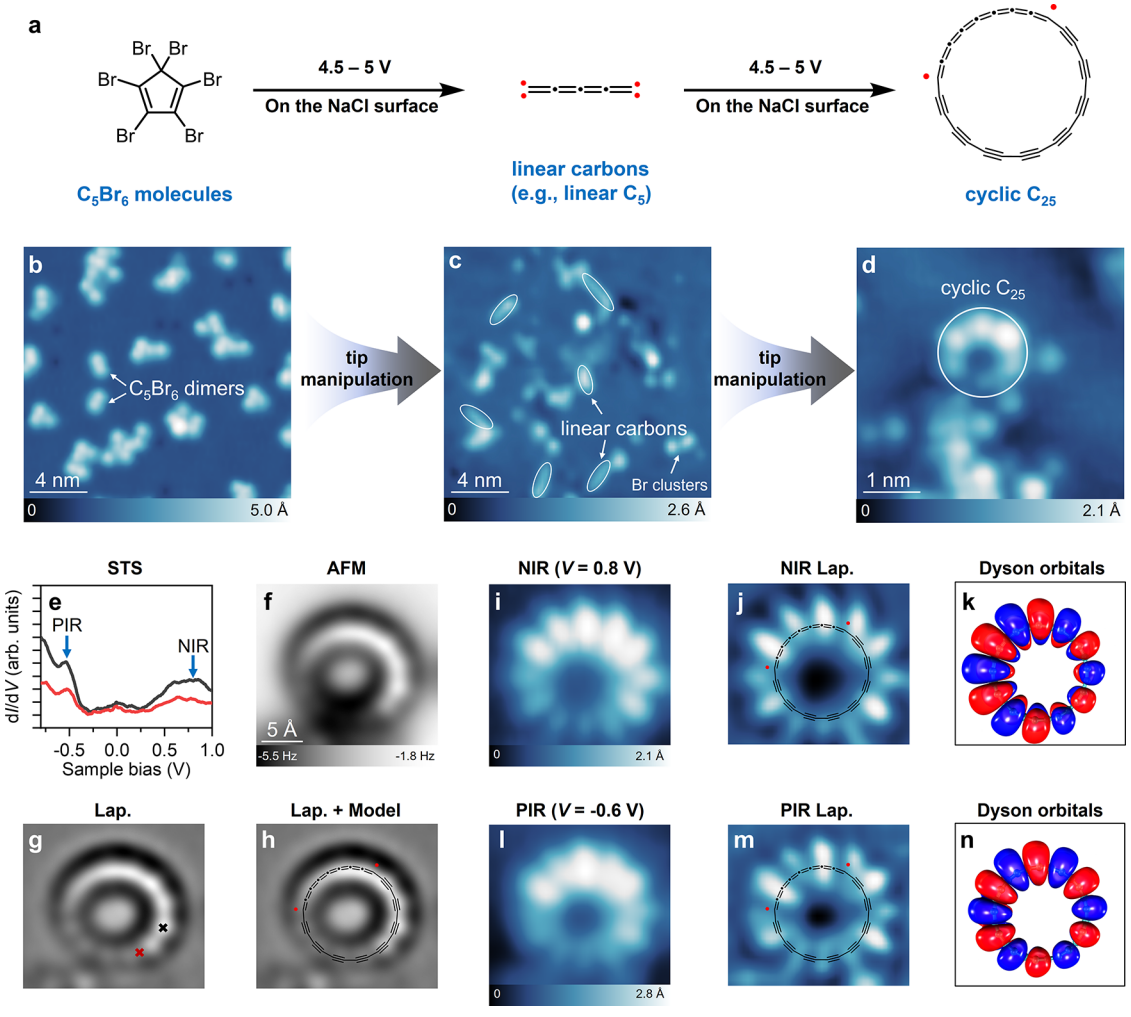

Figure 2. Generation of odd-numbered cyclic C_{25} from linear C_5. (a) Schematic representation of the generation of cyclic C_{25}. (b–d) STM images of C_5Br_6 molecules, generated linear carbons, and cyclic C_{25}. The additional features in (c) and (d) correspond to halogen atoms or reaction intermediates. (e) Scanning tunneling spectroscopy (STS) acquired over triple bond (black cross in g) and single bond (red cross in g) of cyclic C_{25}. The differential conductance (dI/dV) signal shows two peaks that can be attributed to the PIR and NIR states. (f–h) AFM image ($\Delta z = -1.1$ Å) and Laplace-filtered images with superimposed model of cyclic C_{25}. Reference set point of Δz for f: $I = 0.5$ pA, $V = +0.3$ V. STM images (constant-current mode) (i, l) and Laplace-filtered images (j, m) at NIR and PIR of cyclic C_{25} obtained with a CO tip. (k, n) Isosurfaces of Dyson orbitals associated with the processes of electron addition and removal. The orientation of the C_{25} molecule remains the same as in AFM, STM, and calculated images. The scale bar in (f) applies to all STM and AFM images of C_{25}. STM image conditions: $I = 0.5$ pA, $V = +0.3$ V for (b, c), $I = 0.9$ pA, $V = -0.3$ V for (d), $I = 0.9$ pA, $V = +0.8$ V for (i), $I = 0.9$ pA, $V = -0.6$ V for (l).

https://doi.org/10.1021/jacs.6c00225
J. Am. Chem. Soc. XXXX, XXX, XXX–XXX

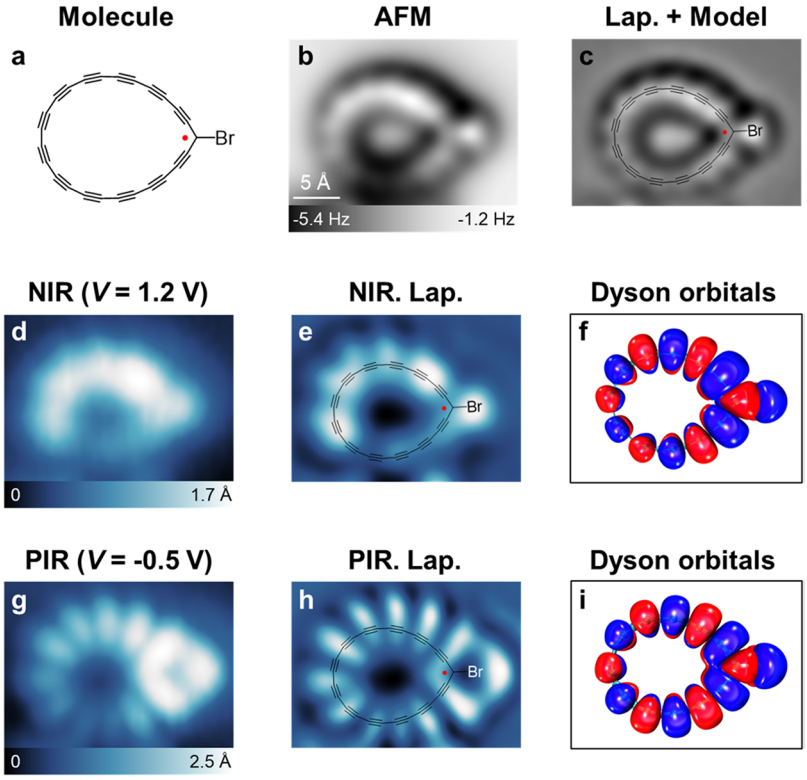

Figure 3. Characterization of $C_{25}Br$. (a–c) Molecule, AFM image ($\Delta z = -1.0$ Å) and Laplace-filtered AFM image with superimposed model of $C_{25}Br$. Reference set point of Δz for b: $I = 0.5$ pA, $V = +0.3$ V. STM images (constant-current mode) and Laplace-filtered images at NIR (d, e) and PIR (g, h) of $C_{25}Br$ obtained with a CO tip. (f, i) Isosurfaces of Dyson orbitals associated with the processes of electron addition and removal. STM image conditions: $I = 1.2$ pA, $V = +1.2$ V for (d), $I = 1.2$ pA, $V = -0.5$ V for (g). The scale bar in (b) applies to all STM and AFM images of $C_{25}Br$.

Scanning tunneling spectroscopy (STS) was performed on cyclic C_{25} to probe its electronic structure. The differential conductance as a function of voltage, dI/dV spectra acquired over the triple bond (black line) and single bond (red line) both show two ion resonances, i.e., positive ion resonance (PIR) and negative ion resonance (NIR) at around −0.54 and +0.8 V, respectively (Figure 2e). STM images at −0.6 and 0.8 V both show 12 characteristic lobes at the same positions around the ring (Figure 2i,j for NIR; Figure 2l,m for PIR). The similar feature of PIR and NIR implies an open-shell electronic structure of C_{25}.[43]

Calculations were performed to obtain the ground-state structure of cyclic C_{25}. As odd-numbered cyclic carbons typically exhibit closely competing singlet and triplet states,[8] to resolve this uncertainty, complete active space self-consistent field (CASSCF) calculations were performed for both spin states of C_{25}. The multiconfigurational analysis demonstrates that C_{25} adopts triplet as the energetically preferred ground state. In addition, the relaxed most stable structure shows a nearly circular geometry with a cumulene-polyyne hybrid structure (Figure S3). AFM simulations (Figure S1) based on this geometry are consistent with experimental AFM images. The frontier orbitals of cyclic C_{25} exhibit two singly occupied orbitals: one is in-plane and the other is out-of-plane, both displaying 12 lobes at equivalent positions around the carbon ring (Figure S4). The in-plane orbital is 0.02 eV higher than the out-of-plane one; that means these two orbitals are nearly energetically degenerate. Thus, we calculated the superposition of these two orbitals (Figure S4) and reproduced well with the 12-lobe patterns observed in the STM images at PIR and NIR. PIR and NIR states should dominantly relate to the out-of-plane singly occupied orbital.[25] In addition, due to the energy broadening of the ionic resonances on NaCl (~0.3 V),[44] nearly degenerated out-of-plane and in-plane orbitals could not be resolved as separate peaks in dI/dV spectra.

To provide a more rigorous representation of electron addition and removal processes occurring in NIR and PIR, Dyson orbitals defined as overlaps between the N-electron ground state and the $(N \pm 1)$-electron state were calculated (Figure 2 and S5). During electron addition (NIR), the extra electron preferentially occupies the lower-energy out-of-plane orbital than the higher-energy in-plane orbital. The energy of the charged molecule with the out-of-plane orbital populated is 0.19 eV lower than that with the in-plane orbital populated. Upon electron removal (PIR), electron extraction preferentially also occurs from the out-of-plane orbital, with the energy being 0.31 eV lower than that for the in-plane orbital. These results are consistent with the observation of the out-of-plane orbital features in both the NIR and PIR.

Cyclic C_{25} can be further functionalized via halogenation, where reaction with a single Br atom yields $C_{25}Br$ (Figure 3a). AFM and Laplace-filtered images (Figure 3b,c) reveal a 25-membered carbon ring containing 12 triple bonds. Calculations indicate that, in contrast to the open-shell triplet ground state of C_{25}, the addition of a Br atom converts the system into an open-shell doublet as the ground state (Figure S6). For the doublet state of $C_{25}Br$, a single frontier orbital is singly occupied near the Fermi level. Thus, both electron addition and removal should involve this orbital, resulting in similar spatial features in the Dyson orbitals (Figure 3f,i). STM and Laplace-filtered images at +1.2 V (Figure 3d,e) and −0.5 V (Figure 3g,h) represent the NIR and PIR states. For PIR, 11

https://doi.org/10.1021/jacs.6c00225
J. Am. Chem. Soc. XXXX, XXX, XXX−XXX

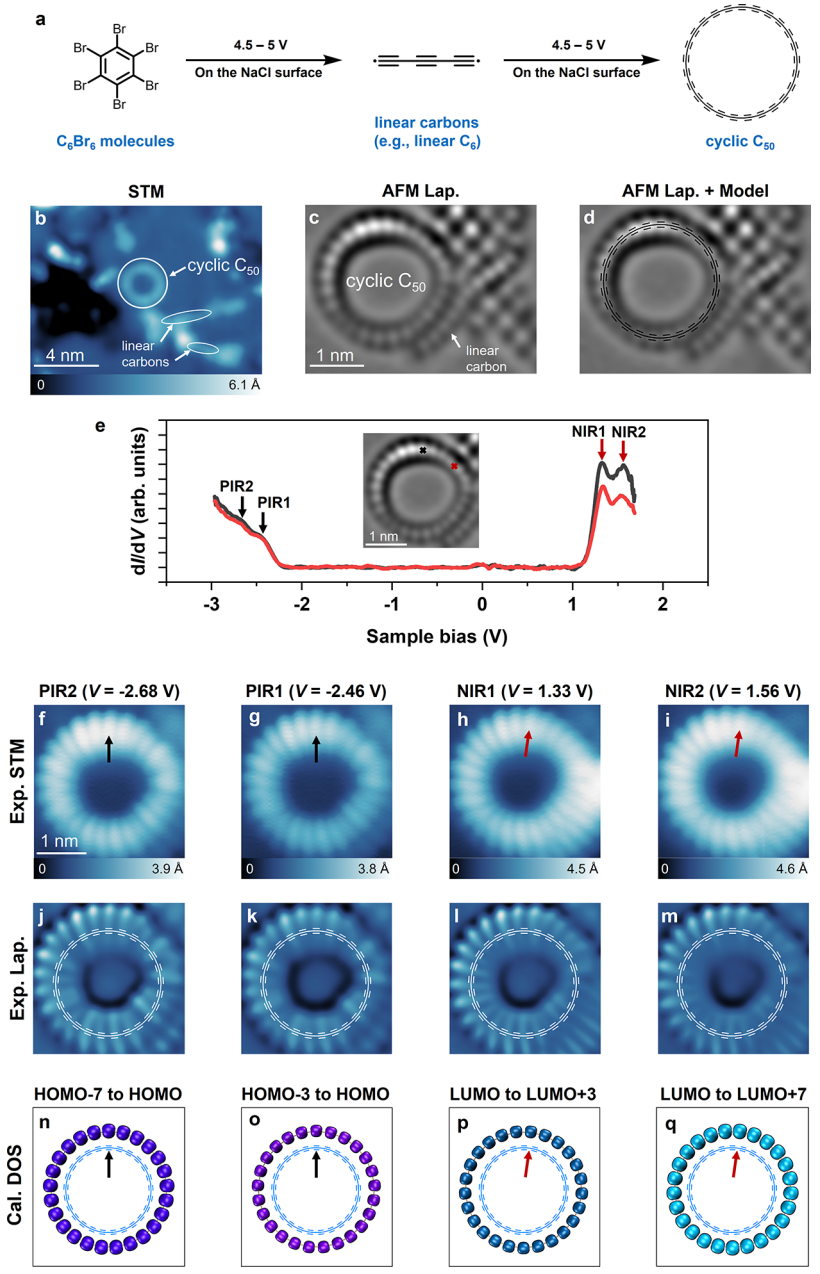

Figure 4. Generation of even-numbered cyclic C_{50} from linear C_6. (a) Schematic representation of the generation of cyclic C_{50}. (b) Large-area STM image. Both linear carbons and cyclic C_{50} are shown. (c, d) Laplace-filtered AFM images with superimposed model of cyclic C_{50}. A linear carbon was also shown. (e) STS acquired over triple bond (black cross in the inset) and single bond (red cross in the inset) of cyclic C_{50}. The differential conductance (dI/dV) signal shows peaks that can be attributed to the PIR and NIR states. STM images (constant-current mode) and corresponding Laplace-filtered STM images at PIR2 (f, j), PIR1 (g, k), NIR1 (h, l), and NIR2 (i, m) of cyclic C_{50} obtained with a CO tip. Black and red arrows indicate the positions of triple and single bonds. (n−q) Corresponding calculated superpositions of frontier orbitals. STM image conditions: I = 2 pA, V = −2.68 V for (f), I = 2 pA, V = −2.46 V for (g), I = 2 pA, V = 1.33 V for (h), I = 2 pA, V = 1.56 V for (i). The scale bar in (c) also applies to (d). The scale bar in (f) applies to all STM images of C_{50}.

lobes are clearly shown around the carbon ring, consistent with the calculated Dyson orbital (Figure 3i). For NIR, the lobes in the lower part cannot be clearly distinguished.

Apart from the occurrence of halogenation reaction of cyclic C_{25}, due to the existence of linear carbons on the surface, we also successfully induced the coupling reaction of cyclic C_{25} with a linear C_{10}, forming a ring-chain "lollipop-shaped" structure (Figure S7). The C_{25} ring in this complex displayed 12 triple bonds, similar to that in $C_{25}Br$.

To demonstrate the generality of this "Ouroboros-inspired" strategy, we employed a longer linear carbon, C_6, aiming to synthesize a larger cyclocarbon (Figure 4a). After the deposition of C_6Br_6 molecules on the surface, upon applying bias voltages up to 5 V, both linear and cyclic products were obtained (Figure 4b). Laplace-filtered AFM images (Figure 4c,d) clearly reveal a ring comprising 25 triple bonds, consistent with a polyynic structure assigned to C_{50}, which is the largest cyclocarbon generated to date. Note that carbon−carbon bonds could be broken in the manipulation processes.[33]

With the help of the Br atoms and a linear carbon aside, the lateral movement of cyclic C_{50} has been suppressed, allowing us to obtain its detailed electronic states. The dI/dV spectra

https://doi.org/10.1021/jacs.6c00225
J. Am. Chem. Soc. XXXX, XXX, XXX−XXX

obtained over triple bond (black line) and single bond (red line) both appear distinct features that can be assigned to the ion resonance states (Figure 4e). Two positive ion resonances (PIR1 and PIR2) are detected at −2.46 and −2.68 V, respectively, and two negative ion resonances (NIR1 and NIR2) appear at +1.33 and +1.56 V. STM images and Laplace-filtered STM images acquired at PIR1/PIR2 and NIR1/NIR2 display 25 lobes distributed over triple bonds (the black arrows indicate the positions of triple bond strictly derived from experimental AFM images, see Figure S8) and single bonds (the red arrows indicate the positions of single bond), respectively (Figure 4f−m), consistent with the orbital distributions observed in the cases of C_{20} and C_{26}.[25,29] Compared with PIR1 and NIR1, PIR2 and NIR2 exhibit a bit larger local density of states.

Calculations show that for cyclic C_{50}, the highest occupied molecular orbitals (HOMO−3 to HOMO) are nearly energetically degenerated. The superposition of these orbitals (Figure 4o) reproduces the experimental STM image of PIR1. Similarly, the superposition of lowest unoccupied orbitals (LUMO to LUMO+3, Figure 4p) corresponds well to the NIR1. In addition, for higher frontier orbitals, the HOMO−7 to HOMO−4 (LUMO+4 to LUMO+7) are also nearly energetically degenerate. Thus, the PIR2 (NIR2) in STM images should arise from the superposition of HOMO−7 to HOMO (Figure 4n) (LUMO to LUMO+7, Figure 4q), respectively (Figure S9).

CONCLUSION

In summary, we have demonstrated a "Ouroboros-style" on-surface synthesis strategy for the formation of cyclic carbons from linear ones, yielding odd- and even-numbered cyclocarbons, namely, C_{25} and C_{50}. High-resolution AFM imaging and calculations revealed that C_{25} adopts a hybrid cumulene−polyyne structure with an open-shell character, while its brominated derivative $C_{25}Br$ exhibits a polyynic configuration and an open-shell doublet state. C_{50} being the largest cyclocarbon generated on the surface so far is characterized as a polyynic structure, whose orbital distributions were well reproduced by DFT calculations. This work opens up another strategy for the synthesis of cyclocarbons directly from linear ones.

EXPERIMENTAL AND THEORETICAL METHODS

Experimental Details for STM and AFM Measurements

STM and AFM measurements were carried out in a commercial (Createc) low-temperature system operated at 4.7 K with a base pressure better than 1×10^{-10} mbar. The single-crystalline Au(111) surface was cleaned by several sputtering and annealing cycles. The NaCl films were obtained by thermally evaporating NaCl crystals onto a clean Au(111) surface at room temperature, resulting in islands of one- and two-monolayer (ML) thickness. The perbromocyclopenta-1,3-diene (C_5Br_6, purchased from Shaanxi Yikunte Pharmaceutical Technology Co., Ltd., 98%) and hexabromobenzene (C_6Br_6, purchased from Adamas-beta, 98%) molecules were separately deposited on cold NaCl/Au(111) surface by thermal sublimation from a molecular evaporator (sublimation temperature: 44 °C for C_5Br_6, 85 °C for C_6Br_6). CO molecules for tip modification[45] were dosed onto the cold sample via a leak valve. We used qPlus sensors[46] with a resonance frequency f_0 = 29.49 kHz, quality factor $Q \approx 45{,}000$, and a spring constant $k \approx 1800$ N/m operating in frequency-modulation mode.[47] The bias voltage V was applied to the sample with respect to the tip. AFM images were acquired in constant-height mode at V = 0 V and an oscillation amplitude of A = 1 Å. The tip-height offsets Δz for constant-height AFM images are defined as the offset in the tip−sample distance relative to the STM set point at the NaCl surface. The positive (negative) values of Δz correspond to the tip−sample distance increased (decreased) with respect to a STM set point. Additional supporting figures are shown in Figures S10 and S11.

Density Functional Theory Calculations

Density functional theory (DFT) calculations were carried out in the gas phase using Gaussian 16 program package.[48] ωB97XD exchange-correlation functional[49] in conjunction with def2-TZVP[50] basis sets was used for calculations of cyclic C_{25} and C_{50} in gas phase.

The AFM simulations were conducted by the PP-AFM code provided by Hapala et al.[51] The detailed parameters are listed below. The lateral spring constant for the CO tip was 0.2 N/m, and a quadrupole-like charge distribution at the tip apex was used to simulate the CO tip with $q = -0.1$ e (e is the elementary charge and refers to $|e|$, and q is the magnitude of quadrupole charge at the tip apex). The amplitude was set as 1 Å. The difference in probe height between "sim. far" and "sim. close" corresponded to the respective difference between "AFM far" and "AFM close."

CASSCF Calculations

All multireference calculations were performed using the OpenMolcas package.[52] The CASSCF method was employed to describe the multiconfigurational character of the systems, and the resulting energies were further refined using CASPT2 corrections.[53,54] The def2-SVP basis set was employed throughout this work.[50] For C_{25}, the active space comprised 8 electrons in 8 molecular orbitals located near the Fermi level, whereas for $C_{25}Br$, the active space included 9 electrons in 10 orbitals.

For geometry optimization, the initial geometries were taken from DFT-optimized structures and subsequently reoptimized at the CASSCF level using the default SLAPAF algorithm implemented in OpenMolcas. When oscillations in the total energy impeded convergence, the keywords C2-DIIS, CARTESIAN, and a reduced MAXSTEP value were applied to stabilize the optimization process, ensuring convergence within 0.02 mHa.

To obtain more accurate frontier orbital energies, single-point calculations were performed at the CASPT2(14,12) and CASPT2-(13,12) levels for C_{25} and $C_{25}Br$, respectively, using the same basis set.

Dyson orbitals were computed using the RASSI module in OpenMolcas based on the optimized geometries.[52,55] For NIR, the Dyson orbitals were obtained from the overlap between the N-electron and (N + 1)-electron wavefunctions, corresponding to electron attachment. In contrast, for PIR, the Dyson orbitals were derived from the overlap between the N-electron and (N − 1)-electron wavefunctions, corresponding to electron detachment.

Molecular orbitals were visualized using a combination of Multiwfn 3.8(dev) code for wavefunction analysis and Visual Molecular Dynamics (VMD) for graphical rendering.[56−58]

ASSOCIATED CONTENT

Data Availability Statement

All data are available in the main text or the Supporting Information.

Supporting Information

The Supporting Information is available free of charge at https://pubs.acs.org/doi/10.1021/jacs.6c00225.

STM images, DFT calculations, and related discussions (PDF)

AUTHOR INFORMATION

Corresponding Authors

Luye Sun − *Interdisciplinary Materials Research Center, School of Materials Science and Engineering, Tongji University, Shanghai 201804, People's Republic of China;*

https://doi.org/10.1021/jacs.6c00225
J. Am. Chem. Soc. XXXX, XXX, XXX−XXX

orcid.org/0000-0003-2678-2517; Email: sunly@tongji.edu.cn

Wei Xu − *Interdisciplinary Materials Research Center, School of Materials Science and Engineering, Tongji University, Shanghai 201804, People's Republic of China;* orcid.org/0000-0003-0216-794X; Email: xuwei@tongji.edu.cn

Authors

Yuan Guo − *Interdisciplinary Materials Research Center, School of Materials Science and Engineering, Tongji University, Shanghai 201804, People's Republic of China*

Ling Hua − *Interdisciplinary Materials Research Center, School of Materials Science and Engineering, Tongji University, Shanghai 201804, People's Republic of China*

Yuzhe Yun − *Interdisciplinary Materials Research Center, School of Materials Science and Engineering, Tongji University, Shanghai 201804, People's Republic of China*

Guorui Xu − *Interdisciplinary Materials Research Center, School of Materials Science and Engineering, Tongji University, Shanghai 201804, People's Republic of China*

Complete contact information is available at: https://pubs.acs.org/10.1021/jacs.6c00225

Author Contributions

†Y.G. and L.H. contributed equally to this work. The manuscript was written through contributions of all authors. All authors have given approval to the final version of the manuscript.

Notes

The authors declare no competing financial interest.

■ ACKNOWLEDGMENTS

The authors acknowledge the financial support from the National Natural Science Foundation of China (22125203, 22402149), the National Key R&D Program of China (2023YFE0101900), the Ministry of Science and Technology of the People's Republic of China, and the Shanghai Science and Technology Program (24ZR1470000).

■ REFERENCES

(1) Hirsch, A. The era of carbon allotropes. *Nat. Mater.* **2010**, *9* (11), 868−871.

(2) Banhart, F. Elemental carbon in the sp^1 hybridization. *ChemTexts* **2020**, *6* (1), No. 3.

(3) Anderson, H. L.; Patrick, C. W.; Scriven, L. M.; Woltering, S. L. A short history of cyclocarbons. *Bull. Chem. Soc. Jpn.* **2021**, *94* (3), 798−811.

(4) Jones, R. O. Density functional study of carbon clusters C_{2n} ($2 \leqslant n \leqslant 16$). I. Structure and bonding in the neutral clusters. *J. Chem. Phys.* **1999**, *110* (11), 5189−5200.

(5) Seenithurai, S.; Chai, J. D. TAO-DFT investigation of electronic properties of linear and cyclic carbon chains. *Sci. Rep.* **2020**, *10* (1), No. 13133.

(6) Zhu, B.-C.; Liu, C.-J.; Deng, P.-J.; Zhao, J.; Zhang, J.; Zeng, L.; Liao, Y.-H.; Bao, L.; Bao, J. DFT-based study on the differences between odd and even C_n (n = 6−31) ring clusters. *Results Phys.* **2023**, *52*, No. 106852.

(7) Brito, B. G. A.; Hai, G. Q.; Cândido, L. Quantum Monte Carlo study on the structures and energetics of cyclic and linear carbon clusters C_n (n = 1,···,10). *Phys. Rev. A* **2018**, *98* (6), No. 062508.

(8) Baryshnikov, G. V.; Valiev, R. R.; Valiulina, L. I.; Kurtsevich, A. E.; Kurten, T.; Sundholm, D.; Pittelkow, M.; Zhang, J.; Agren, H. Odd-number cyclo[n]carbons sustaining alternating aromaticity. *J. Phys. Chem. A* **2022**, *126* (16), 2445−2452.

(9) Furukawa, S.; Fujita, M.; Kanatomi, Y.; Minoura, M.; Hatanaka, M.; Morokuma, K.; Ishimura, K.; Saito, M. Double aromaticity arising from σ- and π-rings. *Commun. Chem.* **2018**, *1* (1), No. 60.

(10) Liu, Z.; Lu, T.; Chen, Q. An sp-hybridized all-carboatomic ring, cyclo[18]carbon: Electronic structure, electronic spectrum, and optical nonlinearity. *Carbon* **2020**, *165*, 461−467.

(11) Liu, Z.; Lu, T.; Chen, Q. An sp-hybridized all-carboatomic ring, cyclo[18]carbon: Bonding character, electron delocalization, and aromaticity. *Carbon* **2020**, *165*, 468−475.

(12) Remya, K.; Suresh, C. H. Carbon rings: a DFT study on geometry, aromaticity, intermolecular carbon−carbon interactions and stability. *RSC Adv.* **2016**, *6* (50), 44261−44271.

(13) Li, M.; Gao, Z.; Han, Y.; Zhao, Y.; Yuan, K.; Nagase, S.; Ehara, M.; Zhao, X. Potential molecular semiconductor devices: cyclo-C_n (n = 10 and 14) with higher stabilities and aromaticities than acknowledged cyclo-C_{18}. *Phys. Chem. Chem. Phys.* **2020**, *22* (8), 4823−4831.

(14) Charistos, N. D.; Muñoz-Castro, A. Induced magnetic field in sp-hybridized carbon rings: analysis of double aromaticity and antiaromaticity in cyclo[2N]carbon allotropes. *Phys. Chem. Chem. Phys.* **2020**, *22* (17), 9240−9249.

(15) Diederich, F. Carbon scaffolding: building acetylenic all-carbon and carbon-rich compounds. *Nature* **1994**, *369* (6477), 199−207.

(16) Baryshnikov, G. V.; Valiev, R. R.; Kuklin, A. V.; Sundholm, D.; Ågren, H. Cyclo[18]carbon: Insight into electronic structure, aromaticity, and surface coupling. *J. Phys. Chem. Lett.* **2019**, *10* (21), 6701−6705.

(17) Liu, M.; Artyukhov, V. I.; Lee, H.; Xu, F.; Yakobson, B. I. Carbyne from first principles: Chain of C atoms, a nanorod or a nanorope. *ACS Nano* **2013**, *7* (11), 10075−10082.

(18) Pitzer, K. S.; Clementi, E. Large molecules in carbon vapor. *J. Am. Chem. Soc.* **1959**, *81* (17), 4477−4485.

(19) Lagow, R. J.; Kampa, J. J.; Wei, H.-C.; Battle, S. L.; Genge, J. W.; Laude, D. A.; Harper, C. J.; Bau, R.; Stevens, R. C.; Haw, J. F.; Munson, E. Synthesis of linear acetylenic carbon: The "*sp*" carbon Allotrope. *Science* **1995**, *267* (5196), 362−367.

(20) Pan, B.; Xiao, J.; Li, J.; Liu, P.; Wang, C.; Yang, G. Carbyne with finite length: The one-dimensional *sp* carbon. *Sci. Adv.* **2015**, *1* (9), No. e1500857.

(21) Parasuk, V.; Almlof, J.; Feyereisen, M. W. The [18] all-carbon molecule: cumulene or polyacetylene? *J. Am. Chem. Soc.* **1991**, *113* (3), 1049−1050.

(22) Arulmozhiraja, S.; Ohno, T. CCSD calculations on C_{14}, C_{18}, and C_{22} carbon clusters. *J. Chem. Phys.* **2008**, *128* (11), No. 114301.

(23) Torelli, T.; Mitas, L. Electron correlation in C_{4N+2} carbon rings: aromatic versus dimerized structures. *Phys. Rev. Lett.* **2000**, *85* (8), 1702−1705.

(24) Kaiser, K.; Scriven, L. M.; Schulz, F.; Gawel, P.; Gross, L.; Anderson, H. L. An sp-hybridized molecular carbon allotrope, cyclo[18]carbon. *Science* **2019**, *365* (6459), 1299−1301.

(25) Albrecht, F.; Roncevic, I.; Gao, Y.; Paschke, F.; Baiardi, A.; Tavernelli, I.; Mishra, S.; Anderson, H. L.; Gross, L. The odd-number cyclo[13]carbon and its dimer, cyclo[26]carbon. *Science* **2024**, *384* (6696), 677−682.

(26) Sun, L.; Guo, Y.; Xiang, W.; Xu, W. On-surface synthesis and characterization of linear and cyclic C_6. *Nat. Synth.* **2025**, *4* (8), 940−946.

(27) Sun, L.; Zheng, W.; Gao, W.; Kang, F.; Zhao, M.; Xu, W. On-surface synthesis of aromatic cyclo[10]carbon and cyclo[14]carbon. *Nature* **2023**, *623* (7989), 972−976.

(28) Gao, Y.; Albrecht, F.; Rončević, I.; Ettedgui, I.; Kumar, P.; Scriven, L. M.; Christensen, K. E.; Mishra, S.; Righetti, L.; Rossmannek, M.; Tavernelli, I.; Anderson, H. L.; Gross, L. On-surface synthesis of a doubly anti-aromatic carbon allotrope. *Nature* **2023**, *623*, 977−981.

(29) Sun, L.; Zheng, W.; Kang, F.; Gao, W.; Wang, T.; Gao, G.; Xu, W. On-surface synthesis and characterization of anti-aromatic cyclo[12]carbon and cyclo[20]carbon. *Nat. Commun.* **2024**, *15* (1), No. 7649.

(30) Scriven, L. M.; Kaiser, K.; Schulz, F.; Sterling, A. J.; Woltering, S. L.; Gawel, P.; Christensen, K. E.; Anderson, H. L.; Gross, L. Synthesis of cyclo[18]carbon via debromination of $C_{18}Br_6$. *J. Am. Chem. Soc.* **2020**, *142* (30), 12921−12924.
(31) Guo, Y.; Yun, Y.; Xiang, W.; Xu, G.; Sun, L.; Xu, W. On-surface synthesis of cyclo[20]carbon and cyclo[30]carbon from cyclo[10]-carbon. *Nat. Commun.* **2025**, *16* (1), No. 11507.
(32) Sun, L.; Guo, Y.; Sahalianov, I.; Zhou, Z.; Zheng, W.; Xiang, W.; Guo, Y.; Feng, Y.; Valiev, R.; Kuklin, A.; Ågren, H.; Baryshnikov, G. V.; Xu, W. Tuning aromaticity of cyclocarbons by heteroatom doping: C12S and C12N. *Natl. Sci. Rev.* **2026**, *13*, No. nwaf472.
(33) Sun, L.; Guo, Y.; Xiang, W.; Zhao, M.; Xu, W. The cumulenic linear C_5 and its coupling-reaction products. *Nat. Commun.* **2025**, *16* (1), No. 9222.
(34) Grutter, M.; Wyss, M.; Riaplov, E.; Maier, J. P.; Peyerimhoff, S. D.; Hanrath, M. Electronic absorption spectra of linear C_6, C_8 and cyclic C_{10}, C_{12} in neon matrices. *J. Chem. Phys.* **1999**, *111* (16), 7397−7401.
(35) Parent, D. C.; McElvany, S. W. Investigations of small carbon cluster-ion structures by reactions with hydrogen cyanide. *J. Am. Chem. Soc.* **1989**, *111* (7), 2393−2401.
(36) McCarthy, M. C.; Thaddeus, P. Microwave and laser spectroscopy of carbon chains and rings. *Chem. Soc. Rev.* **2001**, *30* (3), 177−185.
(37) Van Orden, A.; Saykally, R. J. Small carbon clusters: spectroscopy, structure, and energetics. *Chem. Rev.* **1998**, *98* (6), 2313−2357.
(38) Hoffmann, R. Extended hückel theory—v: Cumulenes, polyenes, polyacetylenes and C_n. *Tetrahedron* **1966**, *22* (2), 521−538.
(39) Liang, C., III; Schaefer, H. F. Carbon clusters: The structure of C_1 studied with configuration interaction methods. *J. Chem. Phys.* **1990**, *93* (12), 8844−8849.
(40) Watts, J. D.; Bartlett, R. J. The nature of monocyclic C_{10}. A theoretical investigation using coupled-cluster methods. *Chem. Phys. Lett.* **1992**, *190* (1−2), 19−24.
(41) Hutter, J.; Luethi, H. P.; Diederich, F. Structures and vibrational frequencies of the carbon molecules C_2-C_{18} calculated by density functional theory. *J. Am. Chem. Soc.* **1994**, *116* (2), 750−756.
(42) Hartwig, J. F. Hydrocarbon synthesis: Ringing the chains. *Nat. Chem.* **2011**, *3* (2), 99−101.
(43) Pavliček, N.; Mistry, A.; Majzik, Z.; Moll, N.; Meyer, G.; Fox, D. J.; Gross, L. Synthesis and characterization of triangulene. *Nat. Nanotechnol.* **2017**, *12* (4), 308−311.
(44) Repp, J.; Meyer, G.; Stojković, S. M.; Gourdon, A.; Joachim, C. Molecules on insulating films: Scanning-tunneling microscopy imaging of individual molecular orbitals. *Phys. Rev. Lett.* **2005**, *94* (2), No. 026803.
(45) Gross, L.; Mohn, F.; Moll, N.; Liljeroth, P.; Meyer, G. The chemical structure of a molecule resolved by atomic force microscopy. *Science* **2009**, *325* (5944), 1110−1114.
(46) Giessibl, F. J. High-speed force sensor for force microscopy and profilometry utilizing a quartz tuning fork. *Appl. Phys. Lett.* **1998**, *73* (26), 3956−3958.
(47) Albrecht, T. R.; Grütter, P.; Horne, D.; Rugar, D. Frequency modulation detection using high-*Q* cantilevers for enhanced force microscope sensitivity. *J. Appl. Phys.* **1991**, *69* (2), 668−673.
(48) Frisch, M. J.; Trucks, G. W.; Schlegel, H. B.; Scuseria, G. E.; Robb, M. A.; Cheeseman, J. R.; Scalmani, G.; Barone, V.; Petersson, G. A.; Nakatsuji, H.; Li, X.; Caricato, M.; Marenich, A. V.; Bloino, J.; Janesko, B. G.; Gomperts, R.; Mennucci, B.; Hratchian, H. P.; Ortiz, J. V.; Izmaylov, A. F.; Sonnenberg, J. L.; Williams; Ding, F.; Lipparini, F.; Egidi, F.; Goings, J.; Peng, B.; Petrone, A.; Henderson, T.; Ranasinghe, D.; Zakrzewski, V. G.; Gao, J.; Rega, N.; Zheng, G.; Liang, W.; Hada, M.; Ehara, M.; Toyota, K.; Fukuda, R.; Hasegawa, J.; Ishida, M.; Nakajima, T.; Honda, Y.; Kitao, O.; Nakai, H.; Vreven, T.; Throssell, K.; Montgomery, J. A., Jr.; Peralta, J. E.; Ogliaro, F.; Bearpark, M. J.; Heyd, J. J.; Brothers, E. N.; Kudin, K. N.; Staroverov, V. N.; Keith, T. A.; Kobayashi, R.; Normand, J.; Raghavachari, K.; Rendell, A. P.; Burant, J. C.; Iyengar, S. S.; Tomasi, J.; Cossi, M.; Millam, J. M.; Klene, M.; Adamo, C.; Cammi, R.; Ochterski, J. W.; Martin, R. L.; Morokuma, K.; Farkas, O.; Foresman, J. B.; Fox, D. J. *Gaussian 16 Rev. C.01*; Gaussian, Inc: Wallingford, CT, 2016.
(49) Chai, J. D.; Head-Gordon, M. Long-range corrected hybrid density functionals with damped atom-atom dispersion corrections. *Phys. Chem. Chem. Phys.* **2008**, *10* (44), 6615−6620.
(50) Weigend, F.; Ahlrichs, R. Balanced basis sets of split valence, triple zeta valence and quadruple zeta valence quality for H to Rn: Design and assessment of accuracy. *Phys. Chem. Chem. Phys.* **2005**, *7* (18), 3297−3305.
(51) Hapala, P.; Kichin, G.; Wagner, C.; Tautz, F. S.; Temirov, R.; Jelínek, P. Mechanism of high-resolution STM/AFM imaging with functionalized tips. *Phys. Rev. B* **2014**, *90* (8), No. 085421.
(52) Galván, I. F.; Vacher, M.; Alavi, A.; Angeli, C.; Aquilante, F.; Autschbach, J.; Bao, J. J.; Bokarev, S. I.; Bogdanov, N. A.; Carlson, R. K.; et al. OpenMolcas: From source code to insight. *J. Chem. Theory Comput.* **2019**, *15* (11), 5925−5964.
(53) Andersson, K.; Malmqvist, PÅ.; Roos, B. O. Second-order perturbation theory with a complete active space self-consistent field reference function. *J. Chem. Phys.* **1992**, *96* (2), 1218−1226.
(54) Roos, B. O.; Taylor, P. R.; Sigbahn, P. E. A complete active space SCF method (CASSCF) using a density matrix formulated super-CI approach. *Chem. Phys.* **1980**, *48* (2), 157−173.
(55) Ortiz, J. V. Dyson-orbital concepts for description of electrons in molecules. *J. Chem. Phys.* **2020**, *153* (7), No. 070902.
(56) Humphrey, W.; Dalke, A.; Schulten, K. VMD: Visual molecular dynamics. *J. Mol. Graphics* **1996**, *14* (1), 33−38.
(57) Lu, T. A comprehensive electron wavefunction analysis toolbox for chemists, Multiwfn. *J. Chem. Phys.* **2024**, *161* (8), No. 082503.
(58) Lu, T.; Chen, F. Multiwfn: a multifunctional wavefunction analyzer. *J. Comput. Chem.* **2012**, *33* (5), 580−592.

https://doi.org/10.1021/jacs.6c00225
J. Am. Chem. Soc. XXXX, XXX, XXX−XXX